Imidazole and Quinoline-Based Promising Agent for Cancer Treatment; Synthesis, Characterization, and Computational Calculations

İmidazol ve Kinolin Bazlı Kanser Tedavisi için Ümit Verici Ajan; Sentezi, Karakterizasyonu ve Bilgisayarsal Hesaplamaları

Tolga Acar YEŞİL[*1] [iD], **Ömer DİLEK**[2] [iD], **Tahir TİLKİ**[3] [iD]

[1] *Sinop University, Türkeli Vocational School, Department of Property Protection and Security, Sinop, Türkiye*
[2] *Isparta University of Applied Sciences, Central Research Laboratory Application and Research Center, Isparta, Türkiye*
[3] *Süleyman Demirel University, Faculty of Engineering and Natural Sciences, Department of Chemistry, Isparta, Türkiye*

Abstract

In this study, a novel imidazole and quinoline-based azo compound (MITPDQ) was synthesized, starting from aniline derivative which was used as an intermediate to synthesize nilotinib, which was used in leukemia treatment, characterized, and its structure was elucidated with spectroscopic techniques such as NMR, FTIR, UV, FTIR, and MS. Theoretical calculations using DFT (B3LYP) method and 6-311G (d,p) basis set were done to obtain optimized geometry and spectral data of MITPDQ. Experimental results were compared with theoretical ones and it was observed that they were compatible with each other. Using the optimized geometry of MITPDQ, the molecular docking studies were also conducted with cancer-related proteins. From docking results, the highest docking score was found to be -11.0 kcal/mol between MITPDQ and 2XIR protein. Also, the ADMET properties of MITPDQ were calculated. From ADMET and docking studies, it was concluded that the MITPDQ has the potential to be a drug candidate after further investigations were done related with this field.

Keywords *Imidazole; Quinoline; Quantum Chemical Calculations; Molecular Docking; ADMET*

Öz

Bu çalışmada lösemi tedavisinde kullanılan nilotinibin sentezinde ara madde olarak kullanılan anilin türevinden yola çıkılarak yeni bir imidazol ve kinolin bazlı azo bileşiği (MITPDQ) sentezlendi ve sentezlenen maddenin yapısı NMR, FTIR, UV, FTIR ve MS gibi tekniklerle karakterize edildi. MITPDQ'nun optimize edilmiş geometrisini ve spektral verilerini elde etmek için DFT (B3LYP) yöntemi ve 6-311G (d,p) temel seti kullanılarak teorik hesaplamalar yapıldı. Deneysel sonuçlar teorik sonuçlarla karşılaştırıldı ve birbirleriyle uyumlu oldukları görüldü. MITPDQ'nun optimize edilmiş geometrisi kullanılarak, kanserle ilişkili proteinlerle de moleküler yerleştirme çalışmaları gerçekleştirildi. Yerleştirme sonuçlarından en yüksek yerleştirme puanının MITPDQ ile 2XIR proteini arasında -11,0 kcal/mol olduğu bulundu. Ayrıca MITPDQ'nun ADMET özellikleri de hesaplandı. ADMET ve Moleküler yerleştirme çalışmalarından bu alanla ilgili ileri araştırmalar yapılarak MITPDQ'nun ilaç adayı olma potansiyeline sahip olduğu sonucuna varıldı.

Anahtar Kelimeler *İmidazol, Kinolin, Kuantum Kimyasal Hesaplamalar, Moleküler Yerleştirme, ADMET*

1. Introduction

Cancer is a worldwide health concern that causes a large amount of death worldwide and It is defined by unchecked cell growth (Rashid et al., 2019). According to the World Health Organization's (WHO) 2020 cancer report, there would be 10 million fatalities and 19.3 million new cases of cancer worldwide. By 2040, there might be an increase to 28.4 million new cases (Sung et al., 2021). Lung cancer, prostate cancer, colorectal cancer, breast cancer, brain tumors, and leukemia are the most prevalent cancer kinds (Siegel et al., 2023). Radiation therapy, chemotherapy, stem cell transplantation, and targeted medicines are currently available for the treatment of cancer (Debela et al., 2021). However, a lot of patients have relapsed or developed resistance to

therapy as a result of these medicines, which frequently have serious adverse effects (Hallek, 2019). There is an immediate requirement for new anticancer therapies that address drug resistance, maximize efficacy, and reduce side effects. Therefore, it is essential to develop novel anticancer medications with improved efficacy and reduced toxicities (Carugo and Draetta, 2019).Heterocyclic rings are a common active pharmacophoric component of authorized medications. In contrast to carbon atoms, heterocyclic molecules have at least one heteroatom, such as nitrogen (N), oxygen (O), or sulfur (S). These compounds play a significant role in organic chemistry. In the field of pharmaceuticals, the large range of heterocyclic ring structures, which make up more than 85% of FDA-approved medicine molecules

(Heravi and Zadsirjan, 2020) provides a distinct advantage as small lead compounds in drug design. Nitrogen containing heterocycles are present in almost 60% of the FDA-approved small medications used to treat cancer (Kumar et al., 2023). Nitrogen-containing heterocycles, such as pyrimidine, pyridine, imidazole, benzimidazole, triazole, indole, and quinoline are used to treat a variety of cancers in addition to covering the cellular targets and biochemical mechanisms of action (Kumar et al., 2023). In heterocyclic chemistry, imidazoles have had a special place, and in recent years, due to their adaptable qualities in chemistry and pharmacology, their derivatives have drawn a lot of attention. Imidazole is a heterocyclic ring composed of nitrogen that has biological and medicinal significance. Imidazole compounds have a wide range of biological activity, including antimicrobial, antitubercular, anticancer, antifungal, and anti-HIV properties (Verma et al., 2013). Quinoline, a planner hetero-aromatic molecule with 10π electrons flowing throughout its structure, has the chemical formula C_9H_7N. Quinoline, a six-membered benzene ring fused with pyridine, is a bicyclic heterocyclic system that is considered a crucial component in the field of medicinal chemistry (Marella et al., 2013). In literature itself makes clear that the various quinoline derivatives have demonstrated outstanding outcomes and possess good biological qualities, including antitubercular, anti-inflammatory, analgesic, cardiotonic, anticancer, antibacterial, antifungal, anthelmintic, and antiprotozoal effects (Yadav and Shah, 2021). The quinoline motif is a key component in the creation of anticancer drugs and is consistently lead in the pharmaceutical industry (Ahadi and Emami, 2020; Akkachairin et al., 2020).

The process of discovering and developing new drugs is difficult and long-consuming, requiring substantial resources in terms of financial, labor, and time (Singh et al., 2023). Unfortunately, a lot of promising compounds fail to produce the expected effects or are found to present unacceptable health hazards to humans, which leads to a high attrition rate in the drug development process. By using ADMET (absorption, distribution, metabolism, elimination, and toxicity) testing, promising pharmacological substances and synthesized new drug candidates are characterized, allowing for the identification of both those with potential and those with significant disqualifying characteristics. The most promising method for drug design and discovery is to use computational approaches for molecular docking and scoring. Compared to traditional approaches, computational drug design and discovery is more affordable, efficient, and productive. 1-[3-Amino-5-(trifluoromethyl)phenyl]-4-methylimidazole is the

precursor to the drug nilotinib, which is given treatment for cancer. Furthermore, this aniline and the compounds derived from it make it a viable substance for further pharmaceutical research and development (Choi et al., 2010; Faudone et al., 2022; Hnatiuk et al., 2022; Jung et al., 2019; Kalinichenko et al., 2019, 2021, 2023; Karabacak Atay et al., 2023; Lu et al., 2015; Pandrala et al., 2022; Zhu et al., 2019). In the light of the information given above, the new azo compound 5-((3-(4-methyl-1H-imidazole-1-yl)-5-(trifluoromethyl)phenyl)diazenyl) quinoline-8-ol (MITPDQ) containing this aniline and quinoline heterocyclic rings was synthesized and characterized by spectroscopic techniques. The quantum chemical calculations were conducted. ADMET properties and Molecular Docking simulations of synthesized compound were investigated by computational techniques.

2. Materials and Methods
### 2.1. General Information

The Merck and Aldrich Chemical Company provided the compounds, which were used without further purification. Aluminum sheets pre-coated with silica gel SIL G/UV254 from MN GmbH & Co. were used to monitor reactions. The spots were made visible in UV light (254 nm). Melting point measurements were determined in an open glass capillary tube using the Stuart SMP 30 melting point instrument. The ^{1}H-NMR was recorded using a 700 MHz Bruker NMR spectrometer. Chemical shifts are reported in terms of parts per million (ppm) of remaining protons in the solvent (DMSO: δ 2.50). The singlet, triplet, quartet, and multiplet NMR peak multiplicities were as follows: s for singlet, d for doublet, t for triplet, and m for multiplet. PG T80+ double-beam spectrophotometer was used to record UV-Vis spectra. A Shimadzu IR Prestige-21 FTIR Spectrometer was used to record the compound's FTIR spectrum in transmission mode at room temperature. The prepared sample was put into an IR cell with a KBr window after being compressed into a self-supporting pellet. The Waters Radıan Asap Direct Mass Detector was used for mass analyses. Full scan acquisition mode, ASAP+/ASAP ionization mode, mass range 100-1200 m/z, cone voltage 10 V, gas (N$_2$), isothermal heater temperature of 600 °C, corona current 3 μA, and capillary dip sampling technique were the analysis methods used.

2.2. Synthesis of MITPDQ compound

According to the procedure described in the literature (Güney et al., 2023). 1-[3-Amino-5-(trifluoromethyl)phenyl]-4-methylimidazole (1, 6.21 mmol; 1.5 g; 1.0 equiv.) was used as the starting material for the synthesis of MITPDQ. In the first step, sodium

nitrite solution (10.87 mmol; 0.75 g; 1.75 equiv.) in 10 mL water and 37% concentrated hydrochloric acid (21.74 mmol; 2.14 g; 1.81 mL; 3.5 equiv.) were used for diazotization of aniline derivative in water that was between -5 and 0 °C. The second step involved the use of coupling reagents (**2,** 6.21 mmol; 0.9 g; 1.0 equiv), ethanol (20 mL), and sodium acetate (62.1 mmol; 5.09 g; 10.0 equiv). **Color:** orange solid. Yield: 89% Mp: 243–245 °C. FTIR (KBR pellet): $\tilde{v}_{max}$ (cm^{-1}) = 3377 (O-H stretching), 2926 (C-H stretching), 1622 (C=C stretching), 1565 (N=N

stretching), 1330 (C=Nstretching), 1156 (C-F stretching). ^{1}H NMR (700 MHz, DMSO): δ = 11.19 (s, 1H), 9.43 (d, *J* = 8.2 Hz, 1H), 9.01 (dd, *J* = 4.0, 1.5 Hz, 1H), 8.50 (d, *J* = 1.3 Hz, 1H), 8.46 (s, 1H), 8.16 (s, 2H), 8.10 (d, *J* = 8.6 Hz, 1H), 7.83 – 7.79 (m, 2H), 7.27 (d, *J* = 8.5 Hz, 1H), 2.20 (d, *J* = 0.9 Hz, 3H). MS = *m/z*: [M+H]$^{+}$ Calcd for $C_{20}H_{15}F_3N_5O$, 398.12; Found: 398.27. Synthesis pathway, reaction parameters, and obtained yield of MITPDQ were depicted in Scheme 1, and The MS spectrum was illustrated in Figure 1.
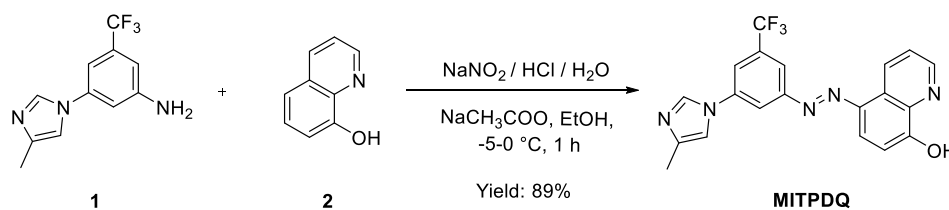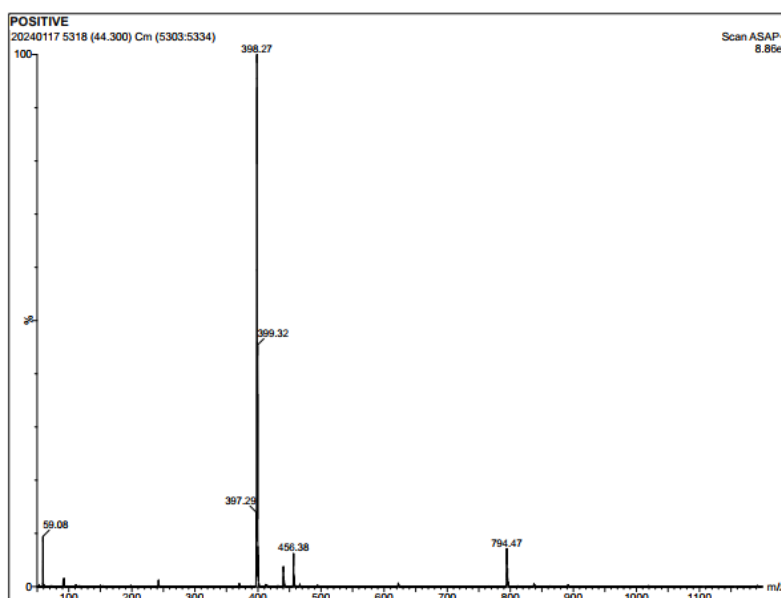

Scheme 1. Synthesis pathway of MITPDQ

Figure 1. Mass spectrum of MITPDQ

2.3. Computational calculations

Theoretical calculations related with quantum chemistry were done by using The Gaussian 09 package (Frish et al., 2016). Chemcraft and Avagadro softwares were used to obtain all visualizations related to quantum chemical computations (Zhurko and Zhurko; Hanwell et al., 2012). The DFT/B3LYP/6-311G(d,p) method was utilized to obtain optimized geometries of MITPDQ (Becke, 1988; Lee et al., 1988). Using the B3LYP functional and the 6-311G(d,p) basis set, the compound's ground state molecular structure was optimized by the application of the DFT approach. For the B3LYP/6–311G(d,p) basis set, the calculated vibrational wavenumbers were scaled as 0.9682 for frequencies over 1700 cm^{-1} and 1.0119 for

frequencies below 1700 cm^{-1} to avoid systematic inaccuracies (Merrick et al., 2007). The TD-DFT (Bauernschmitt and Ahlrichs, 1996; Casida et al., 1998) approach was used to evaluate UV-Vis characteristics, whereas the GIAO approach was used to determine chemical shielding for ^{1}H-NMR (Ditchfield, 1972; Wolinski et al., 1990).

2.4. In silico studies
2.4.1. Molecular Docking Studies

The MITPDQ was subjected to molecular docking investigations using the AutodockVina 1.1.2 software (Trott and Olson, 2009). The BIOVIA Discovery Studio Visualizer (BIOAVIA, 2021) and UCSF Chimera softwares

(Pettersen et al., 2004) were used for all imaging processes. For the molecular docking studies, phosphoinositide 3-kinase (PI3K), Focal Adhesion Kinase (FAK), Vascular Endothelial Growth Factor Receptor 2 Kinase Domain (VEGFR2), and Epidermal Growth Factor Receptor Tyrosine Kinase Domain (EGFR) proteins were chosen. The selected proteins and related PDB IDs were given in Table 1. The protein crystal structures were sourced from Protein Data Bank (Berman, 2000). The

UCSF Chimera program was used to eliminate water and all non-standard residues. Proteins were homologized using the Modeler program before molecular docking studies. A grid box (50 x 50 x 50 Å^3) encircled the active site residues of every protein. The DeepSite module was used for the calculation of three-dimensional binding sites coordinates of the proteins (Jiménez et al., 2017) and the calculated coordinates were depicted in Table 1.

Table 1. 3D Binding site coordinates of cancer-related proteins

Proteins and PDB IDs		Coordinates and Values		
Protein	PDB ID	X	Y	Z
EGFR	1M17	24.8	2.1	51.0
VEGFR2	2XIR	21.0	26.2	38.8
PI3K	1E8X	20.2	64.8	21.8
FAK	1MP8	38.1	-3.6	23.8

2.4.2. ADMET Properties

The ADMETlab 2.0 online service has been used to predict ADMET parameters, including physicochemical, pharmacokinetic, absorption, distribution, metabolism, excretion, and toxicity aspects of the drugs (Xiong et al., 2021). Thus, we used ADMETlab 2.0 web server to estimate the ADMET properties of MITPDQ.

3. Results and Discussions

3.1. Experimental and Computational details
3.1.1. Molecular Structures

To determine the optimal geometry of MITPDQ, a DFT technique using the B3LYP function and 6-311G(d,p) basis set in the gas phase was employed. 2D Optimized geometry of MITPDQ, complete with atom numbering, is shown in Figure 2. Figures 3, 4 presented the compound's FTIR spectra from an experimental and theoretical perspective, and Table 2 displayed FTIR frequencies comparisons between the observed and

expected values for each constituent. The MITPDQ's FTIR spectra revealed the following bands: phenolic -OH at 3377 cm^{-1}, an aromatic C-H at 2926 cm^{-1}, an aromatic alkene C=C at 1622 cm^{-1}, N=N at 1565 cm^{-1}, C-N related with amine group at 1330 cm^{-1}, and C-F at 1156 cm^{-1}. The theoretical calculations indicated the bands; the phenolic -OH at 3590 cm^{-1}, the aromatic C-H at 2933 cm^{-1}, the aromatic alkene C=C at 1623 cm^{-1}, N=N at 1546 cm^{-1}, the aromatic amine C-N at 1332 cm^{-1}, and the C-F at 1187 cm^{-1}.
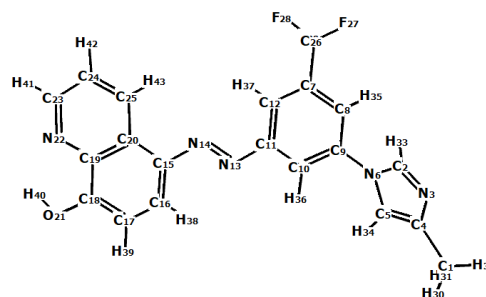

Figure 2. 2D optimized geometry of MITPDQ with atom label
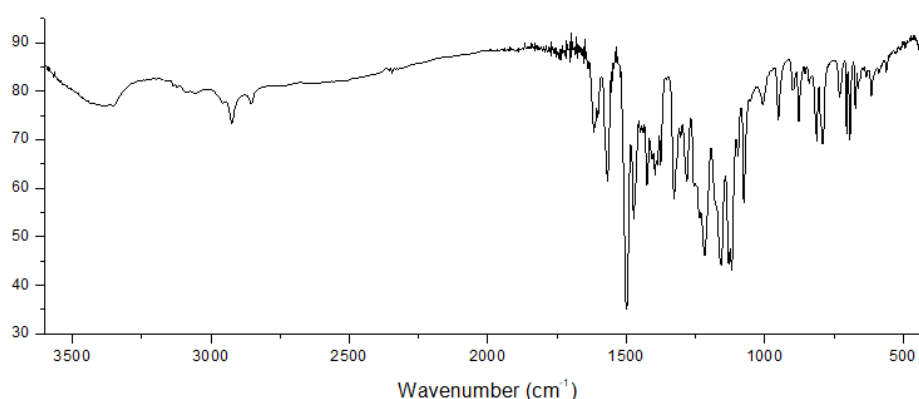
3.1.2. FTIR Spectra

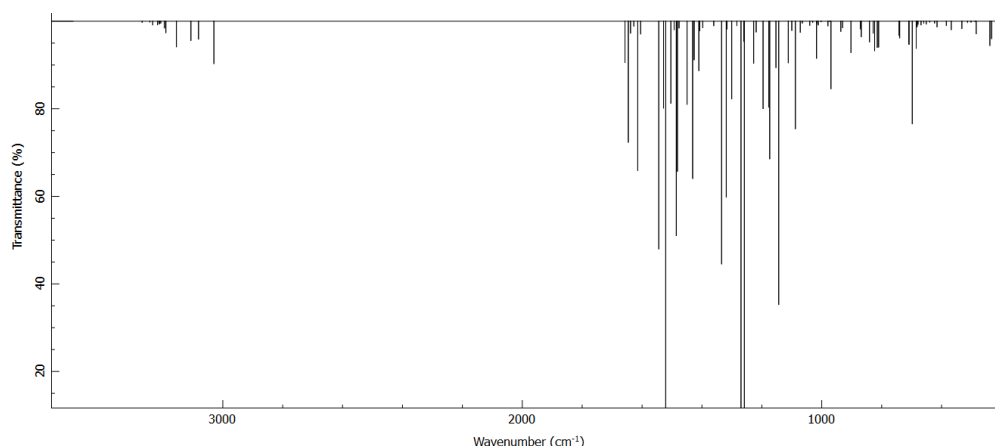**Figure 3.** Experimental FTIR spectrum of MITPDQ

Figure 4. Theoretical FTIR Spectrum of MITPDQ

Table 2. Theoretical and experimental vibrational frequencies of MITPDQ

Vibration	Theoretical	Experimental
O-H stretching	3590	3377
C-H stretching	2933	2926
C=C stretching	1623	1622
N=N bending	1546	1565
C-N stretching	1332	1330
C-F stretching	1187	1156

The linear regression of MITPDQ between the theoretical and experimental frequencies was displayed in Figure 5 and using the DFT/B3LYP method on a molecule, $y = 0.9343x+94.638$ (R^2 = 0.9961) was found to be the equality.
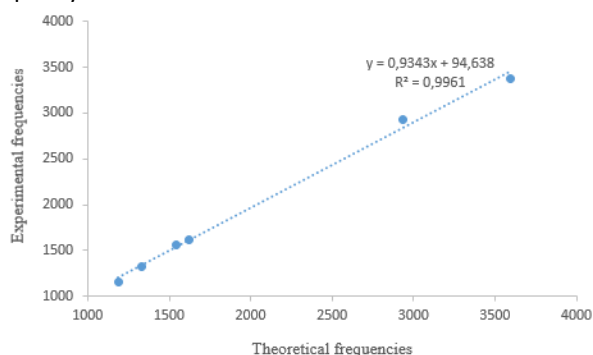

Figure 5. Linearity of experimental and theoretical vibrational frequencies for MITPD

3.1.3. NMR Spectra

The ^{1}H-NMR spectra of MITPDQ related both experimentally and calculated were shown in Figures 6 and 7 respectively. ^{1}H-NMR chemical shift values for MITPDQ were displayed collectively in Table 3 to facilitate comparisons between computed and experimental. The chemical shift value of hydroxy proton (H40) of MITPDQ was lower than the experimental one. The experimental proton chemical shift belong to hydroxyl group of the MITPDQ was observed at 11.19 ppm due to the electronegativity of the nearby oxygen atom (Karabacak Atay et al., 2023) while the theoretical one was 9.04 ppm. The protons related with CH$_3$ group (H30, H31, H32) were found at 2.20 ppm in the experimentally, but they were

found at 2.32-2.19 ppm in theoretically. Aromatic protons (H33, H34, H35, H36, H37, H38, H39, H41, H42, H43) were found to be in the range of 7.27-9.43 ppm experimentally, whereas this range was calculated by the DFT method to be between 7.30-9.66 ppm. The results showed that the experimental values were compatible with theoretical ones.

Table 3. Experimental and Theoretical ^{1}H-NMR chemical shift values of MITPDQ

Label	Theoretical (ppm)	Experimental (ppm)
H43	9.66	9.43
H41	9.11	9.01
H40	9.04	11.19
H38	8.59	8.50
H37	8.44	8.46
H36	8.42	8.16
H42	7.93	
H35	7.78	8.10
H33	7.76	7.83 – 7.79
H39	7.42	
H34	7.30	7.27
H31	2.32	
H32	2.30	2.20
H30	2.19	

3.1.4. UV-Vis spectrum and frontier molecular orbitals

The MITPDQ's UV-vis spectra, which showed three maxima at 270, 412, and 541 nm, was taken in DMSO between 200 and 700 nm. Theoretical electronic transitions were computed using TD-DFT approach and B3LYP/6-311G(d,p) basis set. The theoretical transitions were 293, 296, 317, 327, 332, 409, 423, and 492 nm, respectively. The first electronic transition which was

observed experimentally at 270 nm, was related with π→π*, while the second one at 412 nm, and third one at 541 nm were related with n→π* respectively. It is thought that π→π* transition was related with aromatic ring while n→π* one was related with azo group. The UV-Vis spectra of the MITPDQ in its theoretical and experimental forms were shown in Figures 8, 9. The frontier molecular orbital parameters, such as oscillator strengths (f), excitation energies (eV), and electronic transitions of the MITPDQ were listed in Table 4.
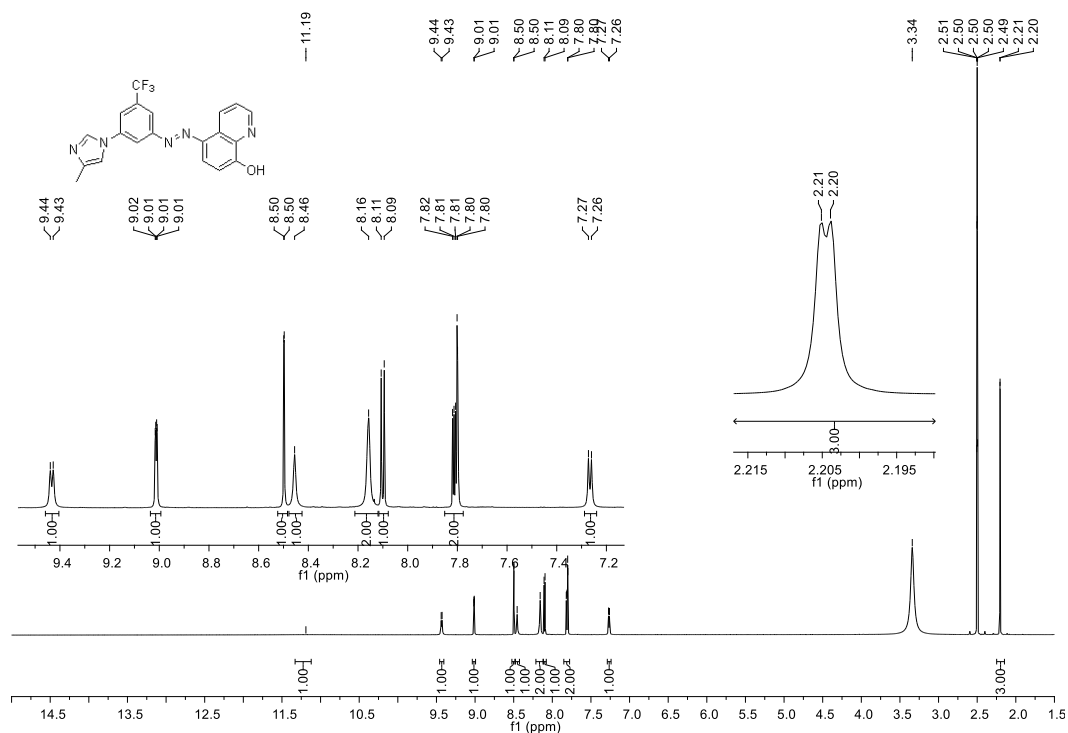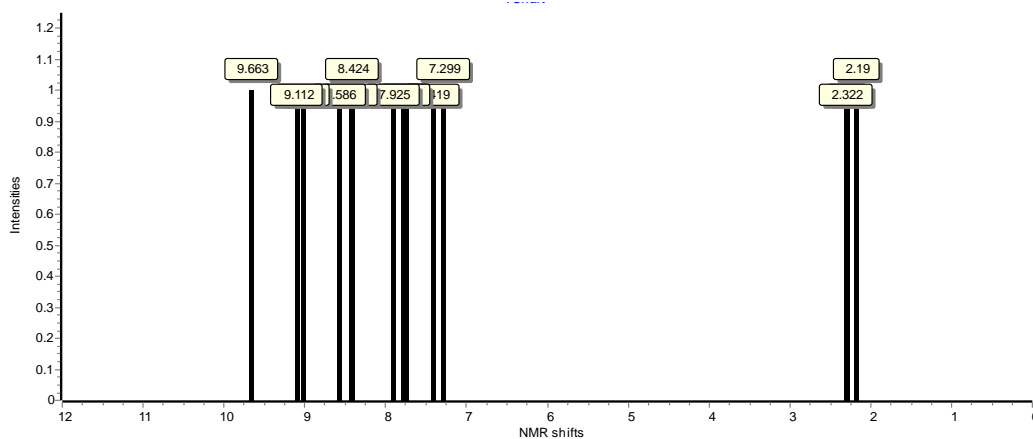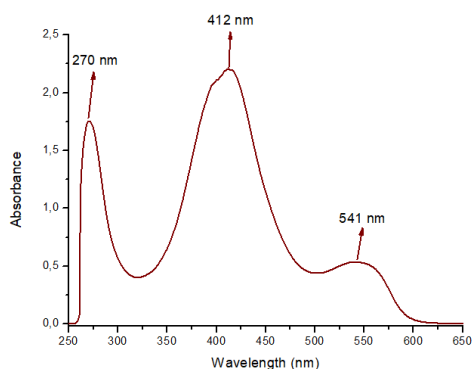

Figure 6. Experimental ^{1}H-NMR spectrum of MITPDQ

Figure 7. Theoretical ^{1}H-NMR spectrum of MITPDQ calculated by GIAO method

Table 4. Experimental and Theoretical Maximum Wavelengths of MITPDQ

Transitions	TD-DFT Maximum Wavelengths (nm)	E (eV)	f	Experimental Maximum Wavelengths (nm)
π→π* (Aromatic ring)	293	4.2302	0.0294	270
	296	4.1856	0.0001	
	317	3.9077	0.0216	
n→π* (-N=N-)	327	3.7889	0.0033	412
	332	3.7348	0.0191	
	409	3.0283	0.1653	
	423	2.9282	0.7511	
n→π*	492	2.5204	0.0022	541

Figure 8. Experimental UV spectrum of MITPDQ
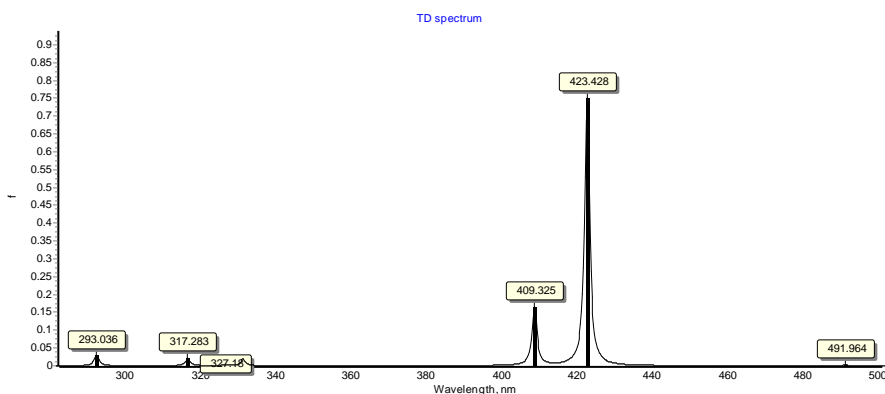
Figure 9. Theoretical UV spectrum of MITPDQ

HOMO and LUMO orbitals are the terms used to describe the border orbitals in compounds. LUMO controls electrophilic reactions in molecules, whereas HOMO controls nucleophilic reactions. HOMO-LUMO orbitals and energies of these orbitals of MITPDQ were computed at the B3LYP/6-311G(d,p) level. Figure 10 provided details on surfaces, the energy difference between HOMO and LUMO, and orbital energies of the MITPDQ. The molecule's HOMO was typically found on the benzene skeletons and imidazole rings, whereas the LUMO was grouped on the benzene skeletons. The HOMO energy of MITPDQ was determined as −6.1357 eV while the LUMO energy was determined as −2.9214 eV. It was discovered that there is 3.2143 eV energy gap between the HOMO and LUMO orbitals. Using the compound's HOMO-LUMO energy values, a number of global reactivity descriptors are listed in Table 5. The MITPDQ's global reactivity parameters were also

determined using the following equations: ionization potential $I = -E_{HOMO}$, electron affinity $A = -E_{LUMO}$, electronegativity $\chi = (I + A)/2$, chemical hardness $\eta = (I - A)/2$, chemical softness $S = 1/2\eta$.
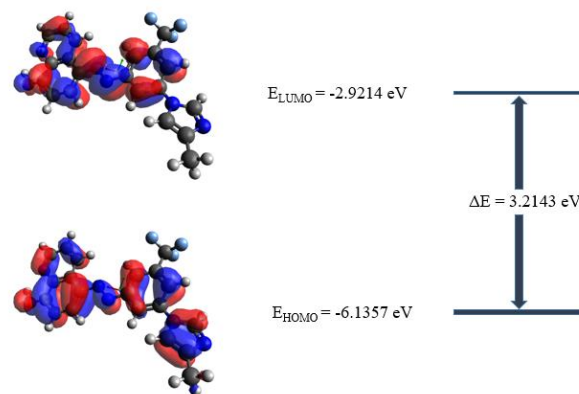
Figure 10. HOMO and LUMO energies of the MITPDQ

Table 5: Global Reactivity Parameters of MITPDQ

Parameter	MITPDQ
E_{HOMO} (eV)	-6.1357
E_{LUMO} (eV)	-2.9214
ΔE (eV)	3.2143
I (eV)	6.1357
A (eV)	2.9214
χ (eV)	4.5286
η (eV)	1.6072
S (eV^{-1})	0.3111

3.2. In silico studies

3.2.1. Molecular docking simulations

The AutodockVina 1.1.2 program was used to conducted molecular docking studies of the MITPDQ. Proteins associated with cancer with PDB IDs of 1M17, 2XIR, 1E8X, and 1MP8 were the subjects of molecular docking investigations. 50 x 50 x 50 Å^3 grid box encircling the active region of the protein and specific protein coordinates (given in Table 1) were used to dock the MITPDQ. The docking scores, which varied from -8.4 kcal/mol to -11.0 kcal/mol, were shown in Table 6. The best docking poses related with the highest docking score of protein-MITPDQ complexes were illustrated in Figure 11, while The 2D visualizations of protein-MITPDQ complexes related with the highest docking score were depicted in Figure 12.

Table 6. Molecular docking results of cancer-related proteins with MITPDQ

PDB ID	Docking Score ΔG : kcal/mol
1M17	-9.2
2XIR	-11.0
1E8X	-9.3
1MP8	-8.4

1E8X-MITPDQ

1M17- MITPDQ
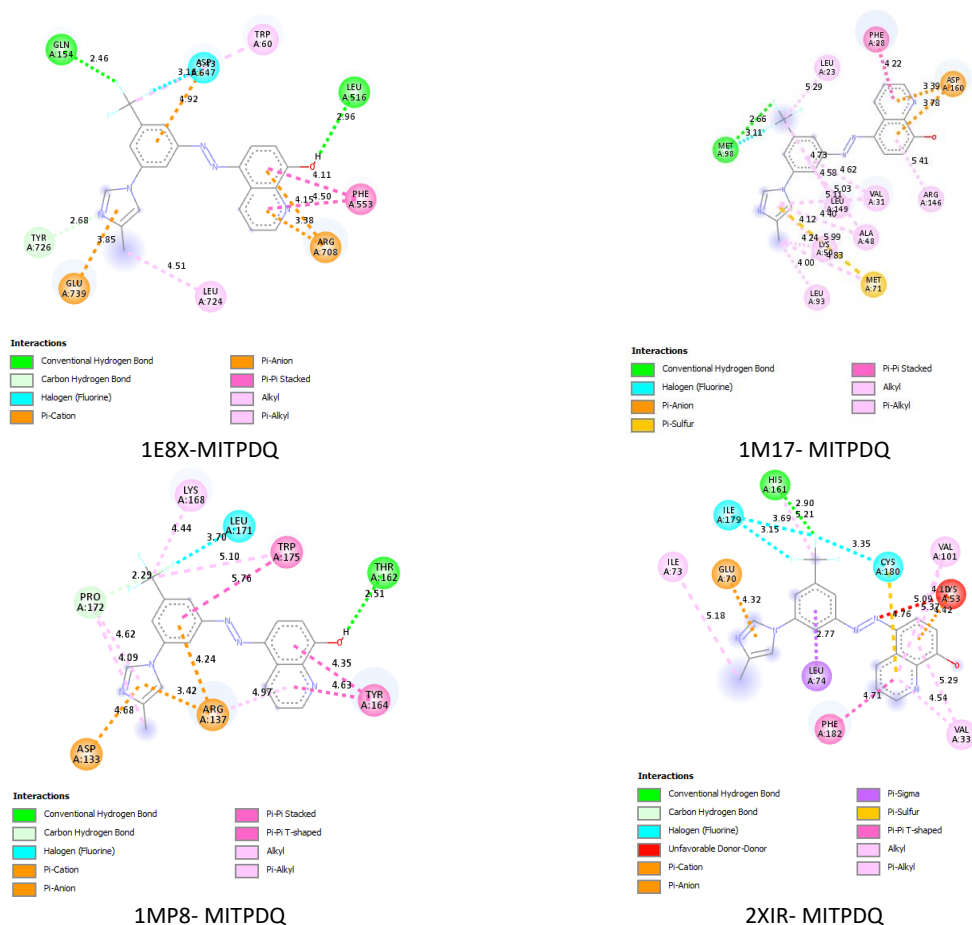

1MP8- MITPDQ

2XIR- MITPDQ

Figure 11. 2D visualization of complexes formed between proteins and MITPDQ

Molecular docking experiments of MITPDQ were conducted independently with 1M17, 2XIR, 1E8X, and 1MP8 proteins. The results showed that the docking scores were -9.2, -11.0, -9.3, and -8.4 kcal/mol, respectively. Analyzing the 1E8X-MITPDQ complex, it was found that interactions between 1E8X and MITPDQ occurred through hydrogen bonds, hydrogen-carbon bonds, halogen, π-anion, π-cation, π-stacked, alkyl, and π-alkyl pairs. There were two hydrogen bonds between the 1E8X protein and the MITPDQ. These bonds have a length of 2.96 Å between LEU516 aminoacid of protein and phenolic -OH and 2.46 Å between GLN154 aminoacid and fluorine atom of the -CF$_3$ group. When the interactions of 1M17 and MITPDQ were examined, It was found that 1M17-MITPDQ complex has one hydrogen bond, halogen, π-anion, π-sulfur, π-stacked, alkyl, and π-alkyl pairs. The hydrogen bond was between fluorine atom of -CF$_3$ group and MET98 with the 2.66 Å bond length. When the interactions between 1MP8 and MITPDQ were examined, there was one hydrogen bond. As well as hydrogen bond, there were carbon-hydrogen bond, halogen, π-cation, π-anion, π-π stacked, π-π-t-shaped, alkyl, and π-alkyl bonds. The hydrogen bond was between hydrogene of phenolic O-H group and THR162 with the 2.51 Å bond length. Upon

examination of the 2XIR complex, it was discovered that interactions took place between 2XIR and MITPDQ via hydrogen bonds, hydrogen-carbon bonds, halogen, π-anion, π-cation, π-σ, π-sulfur, π-π-t-shaped, alkyl, and π-alkyl pairs. Between the MITPDQ ligand and the 2XIR protein, there was one hydrogen bond with a length of 2.90 Å that connected the protein's HIS161 amino acid to the fluorine atom of the CF_3 group.
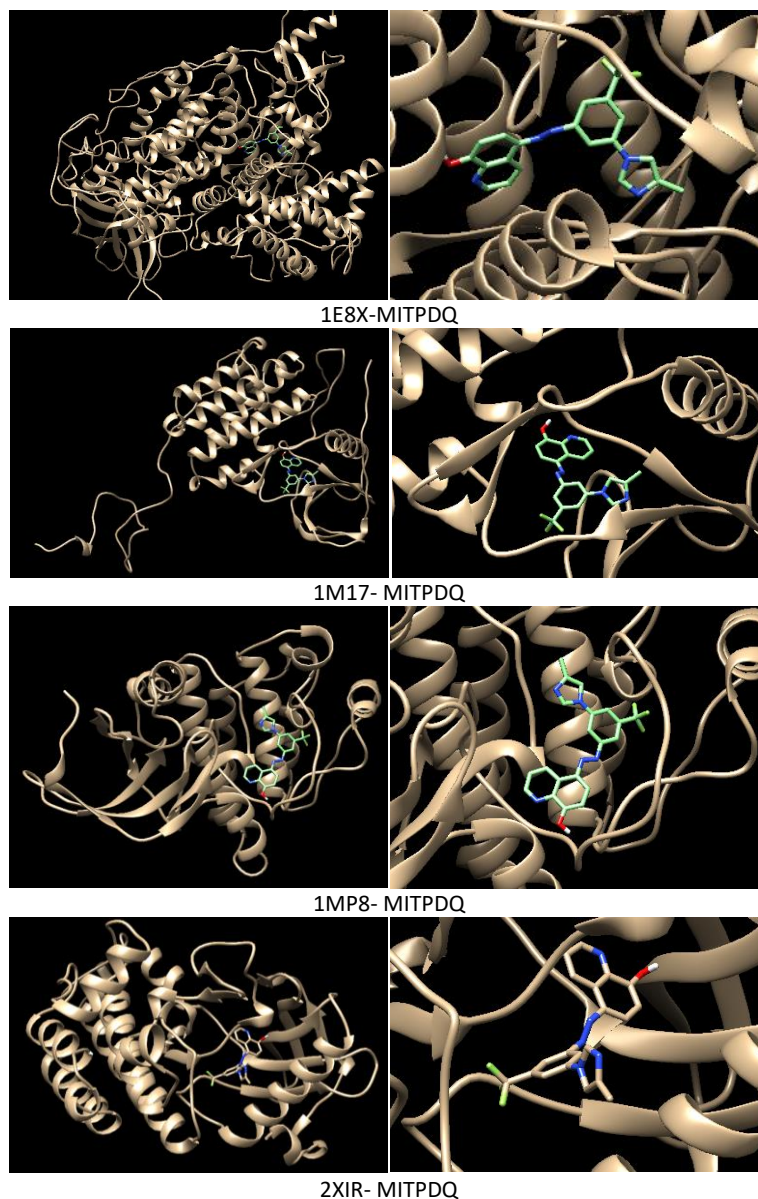

1E8X-MITPDQ

1M17- MITPDQ

1MP8- MITPDQ

2XIR- MITPDQ

Figure 12. 3D visualization of complexes formed between proteins and MITPDQ

3.2.2. ADMET predictions

An important step in the development of any pharmaceutical compound is the identification of ADMET properties. Most candidate chemicals are rejected because of factors such as their inappropriate pharmacokinetics, drug-likeness, etc. The pharmacodynamics and pharmacokinetics of effective and safe medications are precisely balanced to provide high potency, affinity, and selectivity against the molecular target, as well as sufficient ADMET properties (Ferreira and Andricopulo, 2019). Table 7 displays MITPDQ's physicochemical, medicinal chemistry, and ADMET characteristics. The compound's physical characteristics, such as its molecular weight and TPSA

(Topological Polar Surface Area) were investigated. The body's ability to utilize a certain chemical is measured by the TPSA value. The chemical should have a TPSA value of less than 140 Å^2 (Clark, 2000). Following analysis, the compound's TPSA values were discovered to be less than 140 Å². Drug absorption may be impacted by four main parameters, according to Lipinski. These variables include Lipophilicity (Log P), Hydrogen Bond Acceptors (HBA), Hydrogen Bond Donors (HBD), and Molecular Weight (MW) (Lipinski, 2004). Upon analyzing MITPDQ's molecular weight value, it was found to be less than 500, indicating that it was accepted by Lipinski's rule.

Before entering the bloodstream, an oral medication must pass through intestinal cell membranes by active

transport processes, carrier-mediated absorption, or passive diffusion. During the initial stages of drug discovery, the Caco-2 cells that were obtained from human colorectal cancer are frequently utilized to test novel compounds for absorption rate (Bueno, 2015). When the synthesized compound's Caco-2 permeability value was examined, it was found to be more than -5.15. The development of novel pharmacological compounds is significantly hampered by human intestinal absorption (HIA).For the rapid estimation of this property, in silico models that predict the percentage of HIA based on computed molecular descriptors are essential (Hou et al., 2007). Upon analyzing MITPDQ of HIA value (0.004), it was found to possess excellent oral bioavailability. The ability of laboratories to test compounds for mutagenicity was significantly improved by Bruce Ames' bacterial strains and mutagenicity test procedures, which were published in 1973 (Ames et al., 1973). An extended

analysis from the Ames laboratory that followed this publication demonstrated that the test's mutagenicity was a high predictor of carcinogenicity (McCann et al., 1975). AMES toxicity test of MITPDQ revealed an AMES value of 0.34. Assessing the acute toxicity of potential drugs in mammals, such as rats or mice, is a crucial step in ensuring their safety. When the synthesized compound's Oral Acute toxicity value was examined, it was found to be 0.644. Because of its harmful impact on human health, carcinogenicity is one of the most concerning toxicological endpoints of chemical substances. Chemicals may cause cancer because of their ability to damage the genome or disrupt cellular metabolism. Many approved drugs were pulled off the market after it was found that they could cause cancer in humans or animals (Onakpoya et al., 2016). The MITPDQ was found to be non-toxic upon examination of its carcinogenicity values .

Table 7. Calculated ADMET parameters of MITPDQ

Parameters		MITPDQ	Recommended Values
Physicochemical Property	Molecular Formula	$C_{20}H_{14}F_3N_5O$	-
	Molecular Weight (g/mol)	397.12	0-500
	TPSA (Å²)	75.66	0-140
Medicinal Chemistry	Lipinski's Rule	Accepted	Accepted
	SAscore	2.918	≥ 6: difficult <6: easy
Absorption	Caco-2 Permeability	-5.011	>-5.15
	MDCK Permeability	2.1×10^{-5}	$> 20 \times 10^{-6}$
	HIA	0.004	0-0.3: excellent 0.3-0.7: medium 0.7-1.0: poor
Distribution	PPB	97.7%	< 90%
	BBB Penetration	0.012	0-0.3: excellent 0.3-0.7: medium 0.7-1.0: poor
Metabolism	CYP1A2 inhibitor	0.974	
	CYP1A2 substrate	0.758	
	CYP2C19 inhibitor	0.892	
	CYP2C19 substrate	0.071	Category 0: Non-substrate / Non-inhibitor;
	CYP2C9 inhibitor	0.805	
	CYP2C9 substrate	0.429	
	CYP2D6 inhibitor	0.778	Category 1: substrate/inhibitor
	CYP2D6 substrate	0.443	
	CYP3A4 inhibitor	0.786	
	CYP3A4 substrate	0.334	
Excretion	CL	4.105	High: >15 mL/min/kg; moderate: 5-15 mL/min/kg; low: <5 mL/min/kg
	$T_{1/2}$	0.242	0-0.3: excellent 0.3-0.7: medium 0.7-1.0: poor
Toxicity	hERG Blockers	0.584	0-0.3: excellent 0.3-0.7: medium 0.7-1.0: poor
	AMES Toxicity	0.34	
	Rat Oral Acute Toxicity	0.644	
	Carcinogenicity	0.109	

4. Conclusions

Within the scope of study novel imidazole and quinoline-based new azo compound was synthesized and its structure was elucidated with spectroscopic techniques. The quantum chemical calculations were also investigated and it was concluded that theoretical values were compatible with experimental ones. After optimized geometry of MITPDQ was obtained, By using this geometry data, the molecular docking studies were accomplished with cancer related proteins. The docking results were between -8.4 and -11.0 kcal/mol. The highest docking score between 2XIR and MITPDQ. The ADMET parameters were also calculated and the results were examined in terms of to be used as a drug. It was concluded that from ADMET and molecular docking studies, The MITPDQ would to be a drug candidate for cancer treatment after further investigations have been done.

Declaration of Ethical Standards
The authors declare that they comply with all ethical standards.

Credit Authorship Contribution Statement
Author 1: Conceptualization, Investigation, Methodology/Study design, Visualization, Writing – original draft.
Author 2: Conceptualization, Investigation, Methodology/Study design, Visualization, Writing – original draft.
Author 3: Conceptualization, Methodology/Study design, Visualization, Writing – original draft, Writing – review and editing.

Declaration of Competing Interest
The authors declare that they have no known competing financial interests or personal relationships that could have appeared to influence the work reported in this paper.

Data Availability Statement
All data generated or analyzed during this study are included in this published article.

5. References

Ahadi, H., & Emami, S., 2020. Modification of 7-piperazinylquinolone antibacterials to promising anticancer lead compounds: Synthesis and in vitro studies. *European Journal of Medicinal Chemistry*, **187**, 111970. https://doi.org/10.1016/j.ejmech.2019.111970

Akkachairin, B., Rodphon, W., Reamtong, O., Mungthin, M., Tummatorn, J., Thongsornkleeb, C., & Ruchirawat, S., 2020. Synthesis of neocryptolepines and carbocycle-fused quinolines and evaluation of their anticancer and antiplasmodial activities. *Bioorganic Chemistry*, **98**, 103732. https://doi.org/10.1016/j.bioorg.2020.103732

Ames, B. N., Lee, F. D., & Durston, W. E., 1973. An improved bacterial test system for the detection and classification of mutagens and carcinogens. *Proceedings of the National Academy of Sciences of the United States of America*, **70(3)**, 782–786. https://doi.org/10.1073/pnas.70.3.782

Bauernschmitt, R., & Ahlrichs, R., 1996. Treatment of electronic excitations within the adiabatic approximation of time dependent density functional theory. *Chemical Physics Letters*, **256(4–5)**, 454–464. https://doi.org/10.1016/0009-2614(96)00440-X

Becke, A. D., 1988. Density-functional exchange-energy approximation with correct asymptotic behavior. *Physical Review A*, **38(6)**, 3098–3100. https://doi.org/10.1103/PhysRevA.38.3098

Berman, H. M., 2000. The Protein Data Bank. *Nucleic Acids Research*, **28(1)**, 235–242. https://doi.org/10.1093/nar/28.1.235

BIOVIA, 2021 Discovery Studio Visualizer, version 21.1.0.20298. Dassault Systèmes, San Diego, CA.

Bueno, J., 2015. Antimicrobial Models in Nanotechnology. In *Nanotechnology in Diagnosis, Treatment and Prophylaxis of Infectious Diseases* 19–38. Elsevier. https://doi.org/10.1016/B978-0-12-801317-5.00002-5

Carugo, A., & Draetta, G. F., 2019. Academic Discovery of Anticancer Drugs: Historic and Future Perspectives. *Annual Review of Cancer Biology*, **3(1)**, 385–408. https://doi.org/10.1146/annurev-cancerbio-030518-055645

Casida, M. E., Jamorski, C., Casida, K. C., & Salahub, D. R., 1998. Molecular excitation energies to high-lying bound states from time-dependent density-functional response theory: Characterization and correction of the timedependent local density approximation ionization threshold. *The Journal of Chemical Physics*, **108(11)**, 4439–4449. https://doi.org/10.1063/1.475855

Choi, H. G., Ren, P., Adrian, F., Sun, F., Lee, H. S., Wang, X., Ding, Q., Zhang, G., Xie, Y., Zhang, J., Liu, Y., Tuntland, T., Warmuth, M., Manley, P. W., Mestan, J., Gray, N. S., & Sim, T., 2010. A Type-II Kinase Inhibitor Capable of Inhibiting the T315I "Gatekeeper" Mutant of Bcr-Abl. *Journal of Medicinal Chemistry*, **53(15)**, 5439–5448. https://doi.org/10.1021/jm901808w

Debela, D. T., Muzazu, S. G., Heraro, K. D., Ndalama, M. T., Mesele, B. W., Haile, D. C., Kitui, S. K., & Manyazewal, T., 2021. New approaches and procedures for cancer treatment: Current perspectives. *SAGE Open Medicine*, **9**, 205031212110343. https://doi.org/10.1177/20503121211034366

Ditchfield, R., 1972. Molecular Orbital Theory of Magnetic Shielding and Magnetic Susceptibility. *The Journal of Chemical Physics*, **56(11)**, 5688–5691.

https://doi.org/10.1063/1.1677088

Faudone, G., Zhubi, R., Celik, F., Knapp, S., Chaikuad, A., Heering, J., & Merk, D., 2022. Design of a Potent TLX Agonist by Rational Fragment Fusion. *Journal of Medicinal Chemistry*, **65(3)**, 2288–2296. https://doi.org/10.1021/acs.jmedchem.1c01757

Ferreira, L. L. G., & Andricopulo, A. D., 2019. ADMET modeling approaches in drug discovery. *Drug Discovery Today*, **24(5)**, 1157–1165. https://doi.org/10.1016/j.drudis.2019.03.015

Frisch, M. J., G. W., Trucks, H. B., Schlegel, G. E., Scuseria, M. A., Robb, J. R., Cheeseman, G., Scalmani, V., Barone, G. A., Petersson, H., Nakatsuji, X., Li, M., Caricato, A., Marenich, J., Bloino, B. G., Janesko, R., Gomperts, B., Mennucci, H. P., Hratchian, J. V., Ortiz, A. F I., D. J. F. 2016. Gaussian 09, Revision E.01. Gaussian, Inc.

Güney, Y., Dilek, Ö., Sezgin, B., & Tilki, T., 2023. Exploring the Potential of Azo Compounds in Leukemia Treatment: Synthesis and Characterization of New Derivatives with Dimedone and Meldrum's Acid End Groups. *ChemistrySelect*, **8(35)**, e20230264. https://doi.org/10.1002/slct.202302642

Hallek, M., 2019. Chronic lymphocytic leukemia: 2020 update on diagnosis, risk stratification and treatment. *American Journal of Hematology*, **94(11)**, 1266–1287. https://doi.org/10.1002/ajh.25595

Hanwell, M. D., Curtis, D. E., Lonie, D. C., Vandermeersch, T., Zurek, E., & Hutchison, G. R., 2012. Avogadro: an advanced semantic chemical editor, visualization, and analysis platform. *Journal of Cheminformatics*, **4(1)**, 17. https://doi.org/10.1186/1758-2946-4-17

Heravi, M. M., & Zadsirjan, V., 2020. Prescribed drugs containing nitrogen heterocycles: an overview. *RSC Advances*, **10(72)**, 44247–44311. https://doi.org/10.1039/D0RA09198G

Hnatiuk, A. P., Bruyneel, A. A. N., Tailor, D., Pandrala, M., Dheeraj, A., Li, W., Serrano, R., Feyen, D. A. M., Vu, M. M., Amatya, P., Gupta, S., Nakauchi, Y., Morgado, I., Wiebking, V., Liao, R., Porteus, M. H., Majeti, R., Malhotra, S. V., & Mercola, M., 2022. Reengineering Ponatinib to Minimize Cardiovascular Toxicity. *Cancer Research*, **82(15)**, 2777–2791. https://doi.org/10.1158/0008-5472.CAN-21-3652

Hou, T., Wang, J., & Li, Y., 2007. ADME Evaluation in Drug Discovery. 8. The Prediction of Human Intestinal Absorption by a Support Vector Machine. *Journal of Chemical Information and Modeling*, **47(6)**, 2408–2415. https://doi.org/10.1021/ci7002076

Jiménez, J., Doerr, S., Martínez-Rosell, G., Rose, A. S., & De Fabritiis, G., 2017. DeepSite: protein-binding site predictor using 3D-convolutional neural networks. *Bioinformatics*, **33(19)**, 3036–3042. https://doi.org/10.1093/bioinformatics/btx350

Jung, H., Kim, J., Im, D., Moon, H., & Hah, J.-M., 2019. Design, synthesis, and in vitro evaluation of N-(3-(3-alkyl-1H-pyrazol-5-yl) phenyl)-aryl amide for selective RAF inhibition. *Bioorganic & Medicinal Chemistry Letters*, **29(4)**, 534–538. https://doi.org/10.1016/j.bmcl.2019.01.003

Kalinichenko, E., Faryna, A., Bozhok, T., Golyakovich, A., & Panibrat, A., 2023. Novel Phthalic-Based Anticancer Tyrosine Kinase Inhibitors: Design, Synthesis and Biological Activity. *Current Issues in Molecular Biology*, **45(3)**, 1820–1842. https://doi.org/10.3390/cimb45030117

Kalinichenko, E., Faryna, A., Bozhok, T., & Panibrat, A., 2021. Synthesis, In Vitro and In Silico Anticancer Activity of New 4-Methylbenzamide Derivatives Containing 2,6-Substituted Purines as Potential Protein Kinases Inhibitors. *International Journal of Molecular Sciences*, **22(23)**, 12738. https://doi.org/10.3390/ijms222312738

Kalinichenko, E., Faryna, A., Kondrateva, V., Vlasova, A., Shevchenko, V., Melnik, A., Avdoshko, O., & Belko, A., 2019. Synthesis, Biological Activities and Docking Studies of Novel 4-(Arylaminomethyl)benzamide Derivatives as Potential Tyrosine Kinase Inhibitors. *Molecules*, **24(19)**, 3543. https://doi.org/10.3390/molecules24193543

Karabacak Atay, Ç., Dilek, Ö., Tilki, T., & Dede, B., 2023. A novel imidazole-based azo molecule: synthesis, characterization, quantum chemical calculations, molecular docking, molecular dynamics simulations and ADMET properties. *Journal of Molecular Modeling*, **29(8)**, 226. https://doi.org/10.1007/s00894-023-05625-1

Kumar, A., Singh, A. K., Singh, H., Vijayan, V., Kumar, D., Naik, J., Thareja, S., Yadav, J. P., Pathak, P., Grishina, M., Verma, A., Khalilullah, H., Jaremko, M., Emwas, A.-H., & Kumar, P., 2023. Nitrogen Containing Heterocycles as Anticancer Agents: A Medicinal Chemistry Perspective. *Pharmaceuticals*, **16(2)**, 299. https://doi.org/10.3390/ph16020299

Lee, C., Yang, W., & Parr, R. G., 1988. Development of the Colle-Salvetti correlation-energy formula into a functional of the electron density. *Physical Review B*, **37(2)**, 785–789. https://doi.org/10.1103/PhysRevB.37.785

Lipinski, C. A., 2004. Lead- and drug-like compounds: the rule-of-five revolution. *Drug Discovery Today: Technologies*, **1(4)**, 337–341. https://doi.org/10.1016/j.ddtec.2004.11.007

Lu, X., Zhang, Z., Ren, X., Pan, X., Wang, D., Zhuang, X., Luo, J., Yu, R., & Ding, K., 2015. Hybrid pyrimidine alkynyls inhibit the clinically resistance related Bcr-AblT315I mutant. *Bioorganic & Medicinal Chemistry Letters*, **25(17)**, 3458–3463. https://doi.org/10.1016/j.bmcl.2015.07.006

Marella, A., Tanwar, O. P., Saha, R., Ali, M. R., Srivastava, S., Akhter, M., Shaquiquzzaman, M., & Alam, M. M., 2013. Quinoline: A versatile heterocyclic. *Saudi Pharmaceutical Journal*, **21(1)**, 1–12. https://doi.org/10.1016/j.jsps.2012.03.002

McCann, J., Choi, E., Yamasaki, E., & Ames, B. N., 1975. Detection of carcinogens as mutagens in the Salmonella/microsome test: assay of 300 chemicals. *Proceedings of the National Academy of Sciences*, **72(12)**, 5135–5139. https://doi.org/10.1073/pnas.72.12.5135

Merrick, J. P., Moran, D., & Radom, L., 2007. An Evaluation of Harmonic Vibrational Frequency Scale Factors. *The Journal of Physical Chemistry A*, **111(45)**, 11683–11700. https://doi.org/10.1021/jp073974n

Onakpoya, I. J., Heneghan, C. J., & Aronson, J. K., 2016. Post-marketing withdrawal of 462 medicinal products because of adverse drug reactions: a systematic review of the world literature. *BMC Medicine*, **14(1)**, 10. https://doi.org/10.1186/s12916-016-0553-2

Pandrala, M., Bruyneel, A. A. N., Hnatiuk, A. P., Mercola, M., & Malhotra, S. V., 2022. Designing Novel BCR-ABL Inhibitors for Chronic Myeloid Leukemia with Improved Cardiac Safety. *Journal of Medicinal Chemistry*, **65(16)**, 10898–10919. https://doi.org/10.1021/acs.jmedchem.1c01853

Pettersen, E. F., Goddard, T. D., Huang, C. C., Couch, G. S., Greenblatt, D. M., Meng, E. C., & Ferrin, T. E., 2004. UCSF Chimera - A visualization system for exploratory research and analysis. *Journal of Computational Chemistry*, **25(13)**, 1605–1612. https://doi.org/10.1002/jcc.20084

Rashid, H. ur, Xu, Y., Muhammad, Y., Wang, L., & Jiang, J., 2019. Research advances on anticancer activities of matrine and its derivatives: An updated overview. *European Journal of Medicinal Chemistry*, **161**, 205–238. https://doi.org/10.1016/j.ejmech.2018.10.037

Siegel, R. L., Miller, K. D., Wagle, N. S., & Jemal, A., 2023. Cancer statistics, 2023. *CA: A Cancer Journal for Clinicians*, **73(1)**, 17–48. https://doi.org/10.3322/caac.21763

Singh, N., Vayer, P., Tanwar, S., Poyet, J.-L., Tsaioun, K., & Villoutreix, B. O., 2023. Drug discovery and development: introduction to the general public and patient groups. *Frontiers in Drug Discovery*, **3**, 1201419.

https://doi.org/10.3389/fddsv.2023.1201419

Sung, H., Ferlay, J., Siegel, R. L., Laversanne, M., Soerjomataram, I., Jemal, A., & Bray, F., 2021. Global Cancer Statistics 2020: GLOBOCAN Estimates of Incidence and Mortality Worldwide for 36 Cancers in 185 Countries. *CA: A Cancer Journal for Clinicians*, **71(3)**, 209–249. https://doi.org/10.3322/caac.21660

Trott, O., & Olson, A. J., 2009. AutoDock Vina: Improving the speed and accuracy of docking with a new scoring function, efficient optimization, and multithreading. *Journal of Computational Chemistry*, **31(2)**, 455-461. https://doi.org/10.1002/jcc.21334

Verma, A., Joshi, S., & Singh, D., 2013. Imidazole: Having Versatile Biological Activities. *Journal of Chemistry*, **2013**, 1–12. https://doi.org/10.1155/2013/329412

Wolinski, K., Hinton, J. F., & Pulay, P., 1990. Efficient implementation of the gauge-independent atomic orbital method for NMR chemical shift calculations. *Journal of the American Chemical Society*, **112(23)**, 8251–8260. https://doi.org/10.1021/ja00179a005

Xiong, G., Wu, Z., Yi, J., Fu, L., Yang, Z., Hsieh, C., Yin, M., Zeng, X., Wu, C., Lu, A., Chen, X., Hou, T., & Cao, D., 2021. ADMETlab 2.0: an integrated online platform for accurate and comprehensive predictions of ADMET properties. *Nucleic Acids Research*, **49(W1)**, W5–W14. https://doi.org/10.1093/nar/gkab255

Yadav, P., & Shah, K., 2021. Quinolines, a perpetual, multipurpose scaffold in medicinal chemistry. *Bioorganic Chemistry*, **109**, 104639. https://doi.org/10.1016/j.bioorg.2021.104639

Zhu, D., Huang, H., Pinkas, D. M., Luo, J., Ganguly, D., Fox, A. E., Arner, E., Xiang, Q., Tu, Z.-C., Bullock, A. N., Brekken, R. A., Ding, K., & Lu, X., 2019. 2-Amino-2,3-dihydro-1H-indene-5-carboxamide-Based Discoidin Domain Receptor 1 (DDR1) Inhibitors: Design, Synthesis, and in Vivo Antipancreatic Cancer Efficacy. *Journal of Medicinal Chemistry*, **62(16)**, 7431–7444. https://doi.org/10.1021/acs.jmedchem.9b00365

Zhurko, G. A. and Zhurko, D. A. ChemCraft, Tool for treatment of the chemical data, version 1.8; www.chemcraftprog.com